

Preparation and characterization of sub-20 nm Cu_x@Ag₁ core-shell nanoparticles by changing concentration of silver precursor



Sang-Soo Chee, Jong-Hyun Lee*

Department of Materials Science and Engineering, Seoul National University of Science and Technology, Seoul, 139-743, Republic of Korea

HIGHLIGHTS

- Ultrafine Ag-coated Cu nanoparticles less than 20 nm in diameter were fabricated.
- Different Ag precursor concentrations influenced thickness and density of Ag shell.
- Excessive Ag precursor concentrations induced formation of surplus fine pure NPs.
- Ag dewetting behavior and Cu oxidation in Cu₄@Ag₁ nanoparticles were observed.
- Electrical resistivities of sintered Cu₄@Ag₁ films were 2.70–4.96 × 10⁻³ Ω cm.

ARTICLE INFO

Article history:

Received 24 August 2015

Received in revised form

17 September 2016

Accepted 15 October 2016

Available online 18 October 2016

Keywords:

Nanostructures

Chemical synthesis

Electron microscopy

Electrical conductivity

ABSTRACT

Ultrafine Ag-coated Cu (Cu@Ag) nanoparticles (NPs) less than 20 nm in diameter were prepared. After synthesizing ultrafine Cu NPs using a solvothermal method to serve as the core particles, Cu@Ag NPs were fabricated with different initial Ag precursor concentrations, resulting in different thicknesses, densities, and uniformities of Ag shells. The average thickness and density of the Ag shell increased with increasing initial Ag precursor concentration in a Cu:Ag atomic ratio from 6:1 to 1:1. However, excessive Ag precursor concentrations induced homogeneous nucleation and growth of surplus fine pure NPs. Ag dewetting behavior and Cu oxidation in the Cu₄@Ag₁ NPs were observed, they occurred during heating at 200 and 250 °C, respectively. The electrical resistivities of sintered Cu₄@Ag₁ films decreased with increasing temperature from 200 to 240 °C. The resistivity after washing the OA and sintering for 60 min at 240 °C in air was measured to be 4.96 × 10⁻³ Ω cm. The film was sintered in nitrogen using the ink containing non-washed Cu₄@Ag₁ NPs indicated the lower resistivity of 2.70 × 10⁻³ Ω cm owing to the non-oxidation atmosphere, although the chemically capped oleylamine in the core-shell NPs hindered the sintering behavior.

© 2016 Elsevier B.V. All rights reserved.

1. Introduction

Ag nanoparticles (NPs) have been extensively used as conductive inkjet printing inks because of inherently lower resistance and nature of their conductive oxide as compared to other metal NPs [1–6]. Nevertheless, Ag is cost-ineffective and thus still causes bottlenecks in the inkjet printing technology market. In this regard, Cu NPs are excellent alternative materials to Ag because their resistance is similar to that of Ag and they are very inexpensive. However, Cu NPs are vulnerable to surface oxidation in air [7–9]. Hence, methods of fabricating Ag-coated Cu (Cu@Ag) NPs have

been recently studied by many researchers in order to reduce the material cost while preventing Cu oxidation [9–13]. Also, it was recently reported that Ag agglomerates form on Cu surface through Ag dewetting during heating as a result of the unstable interfacial energy, which induces oxidation of exposed pure Cu [12–14]. Consequently, it is important to determine the optimum thickness of a Ag shell and anneal the ink under optimal sintering conditions in order to suppress the Ag dewetting behavior and the conductivity degradation in the Cu@Ag film sintered in air [15–17].

In this study, ultrafine Cu@Ag NPs several tens of nanometers in size, which can be applied to ink-jet printing, were prepared with different Ag shell thicknesses using a solvothermal method for the synthesis of core Cu NPs and an immersion-coating process to prepare thicker and more uniform Ag coatings on the Cu NPs. Then, the Ag dewetting behavior and Cu oxidation were analyzed using

* Corresponding author.

E-mail address: pljh@snut.ac.kr (J.-H. Lee).

the samples with the thickest and most uniform Ag shell, and the electrical resistivities of sintered Cu@Ag films were measured with respect to different sintering conditions.

2. Experimental procedures

For synthesizing core Cu NPs, a solvothermal method using oleylamine (OA, 70%, Aldrich Co.) was employed for 3 h at 240 °C in a nitrogen atmosphere. The detailed synthesis conditions were reported in a previous paper [17]. The synthesis of Cu@Ag core-shell NPs was carried out using a Ag immersion-coating process conducted at 150 °C using varying Ag precursor (silver nitrate, AgNO₃, 99.9%, Kojima Chemicals) concentrations. The Ag precursor was added to 30 mL of OA and allowed to dissolve for 1 h at 60 °C. The added amount of Ag precursor was determined based on Cu:Ag atomic ratios of 6:1–1:1. The completely dissolved solution was then poured into another 100 mL OA solution containing 0.23 g of pure Cu NPs. This mixed solution was heated for 2 h at 150 °C under N₂ bubbling and stirring. Eventually, the color of the solution changed from reddish-brown to yellowish-red. This solution was cooled down for 1 h at room temperature with continual stirring. After the Ag coating, the OA was repetitively exchanged with ethanol (99.9%, Ducksan Chemical Co.) via centrifugation at 10,000 rpm (167 s⁻¹) for 10 min several times in order to remove unnecessary ionic impurities and excess OA in the final NPs. After drying of the Cu@Ag NPs, X-ray diffraction (XRD, X'pert PRO-MPD, PANalytical) analysis was applied to confirm qualitatively the experimental amount ratios between Cu and Ag in the Cu@Ag NPs synthesized with different Cu:Ag atomic ratios. The XRD measurement was carried out in the 2θ range of 20–80° using Cu Kα radiation.

In order to examine the sizes and morphologies of the Cu@Ag NPs, transmission electron microscopy (TEM, Tecnai G² F30ST, FEI Company) was conducted at 300 kV. Formation of fine pure Ag NPs in the Cu@Ag samples was preferentially identified by analyzing the TEM image and using energy dispersive x-ray spectroscopy (EDS) equipped on a TEM. Fast Fourier transformation (FFT) analyses of TEM images were also carried out to determine the phases existed. In addition, scanning transmission electron microscopy (STEM) was performed to analyze the elemental distribution of Cu and Ag according to the same conditions that were used in TEM. The TEM and STEM samples were prepared by adding and drying a droplet of the ethanol solution containing Cu@Ag NPs on a molybdenum grid. The TEM and STEM samples were heated up to 250 °C under air to analyze the metallurgical reactions between the Cu@Ag NPs occurring on a nanoscale with respect to the increase in temperature. In order to observe the sintered properties of the Cu@Ag NPs, moreover, the microstructures of the sintered films were observed using field-emission scanning electron microscopy (FE-SEM, JSM-6700F, JEOL Ltd.).

The films were fabricated via thermal sintering at specific temperature after dropping 1 mL of an ethanol ink containing the 10 wt% Cu@Ag NPs on a 10 × 10 mm silicon wafer. The sintering was performed under air or N₂ atmosphere. Some Cu@Ag NPs were used for the ink material after washing with acetic acid in order to remove chemically capped OA on the NPs. The electrical resistivities of the films with respect to the sintering parameters were measured using a four-point probe (Model 2400, Keithley Instruments Inc.) method.

3. Results and discussion

Fig. 1 shows the TEM images and a selected area electron diffraction (SAED) pattern of Cu@Ag NPs synthesized for 2 h at 150 °C with Cu:Ag atomic ratio of 4:1. The size of the spherical

Cu@Ag NPs ranged from 11.0 to 17.8 nm, and the average diameter and standard deviation were 14.5 and 1.9 nm, respectively. The average diameter of the core Cu NPs was 11.6 nm and the standard deviation was within 2.0 nm [17]. Thus, 2.9 nm, the difference between 14.5 and 11.6 nm, can be considered double the coated Ag-shell thickness. When the size of the spherical Cu NP was 11.6 nm, it was estimated that the size of Cu@Ag NP synthesized with Cu:Ag atomic ratio of 4:1 was 12.9 nm, indicating that the average Ag-shell thickness was just 0.63 nm. Hence, the measured average size of Cu@Ag NPs showed a discrepancy. Given that the actual shapes of the core Cu and Cu@Ag particles were not perfect spherical, the resultant average sizes of the Cu@Ag NPs were slightly higher because the average Ag-shell thickness increased according to the decrease in the surface area. In addition, this discrepancy was attributed to the agglomeration between fabricated Cu@Ag NPs which caused the decrease in the surface area to be plated, as shown in the TEM image of Fig. 1. However, the nearly identical standard deviation value indicates uniformity of the Ag coating. In the high-magnified image of Fig. 1(b), organic capping layers which may be judged as OA were observed. The SAED pattern did not indicate any oxide phases other than pure Cu and Ag, which confirms that Cu was not oxidized during the Cu synthesis and Ag coating under N₂ bubbling.

In order to confirm formation of the core-shell NPs, STEM elemental line profile analysis was carried out and two results are shown in Fig. 2. The ratios between the Ag and Cu counts were the highest at the edges of the profiles and the profiles showed nearly bilateral symmetry. These results confirm the presence of a Ag coating layer on a Cu core NP and the uniformity of the Ag coating.

Fig. 3 shows the TEM and STEM elemental mapping images of Cu@Ag NPs synthesized for 2 h at 150 °C with a Cu:Ag atomic ratio of 2:1. With increasing Ag precursor amount, fine pure Ag NPs several nanometers in diameter were observed in addition to the Cu@Ag NPs, as shown in the TEM image of Fig. 3(a). It can be inferred that the NPs were synthesized through homogeneous nucleation and growth from the excessive amount of initial Ag precursor. It can be easily observed by the elemental mapping images of Fig. 3(b) that the fine NPs are a pure Ag phase. The fine NPs observed in the STEM image indicated detection of the highest Ag intensity, whereas Cu was scarcely detected. The elemental line profiles of another particle in this sample (Fig. 4) also confirm the formation of fine pure Ag NPs. The Ag profile did not show bilateral symmetry, unlike the results shown in Fig. 2, and an intensive Ag count was observed at one edge of the particle. Along with the existence of a fine NP observed in the high-magnified STEM image of Fig. 4(a), the result confirmed the formation of fine Ag NPs.

Fig. 5 presents the elemental mapping images of Cu@Ag NPs synthesized for 2 h at 150 °C with different Cu:Ag atomic ratios. With decreasing Cu:Ag atomic ratio from 6:1 to 1:1, achieved by increasing the initial amount of Ag precursor (AgNO₃), the Ag shell generally became gradually thicker and denser. In the case where the Cu:Ag atomic ratio was 6:1 [Fig. 5(a)], some Ag shells did not cover the Cu surfaces completely, implying a deficiency of Ag atoms. However, thicker and denser Ag shells covered the Cu surfaces and the shell uniformity was also fair in the cases where the Cu:Ag atomic ratio was 5:1 [Fig. 5(b)] or 4:1 [Fig. 5(c)]. In the Cu@Ag NPs synthesized with Cu:Ag atomic ratio of 5:1, the average Ag-shell thickness was calculated as 0.51 nm. In the cases where the Cu:Ag atomic ratio was 3:1 [Fig. 5(d)], 2:1 [Fig. 5(e)], or 1:1 [Fig. 5(f)], meanwhile, Ag mapping in the Ag shell regions became gradually nonuniform. In the cases where the Cu:Ag atomic ratio was 2:1 [Fig. 5(e)] or 1:1 [Fig. 5(f)], moreover, Ag mapping was clearly detected, even when Cu mapping indicated an absence of Cu, indicating that fine pure Ag NPs were synthesized. Therefore, the aim of preparing the thickest and most uniform Ag shells could

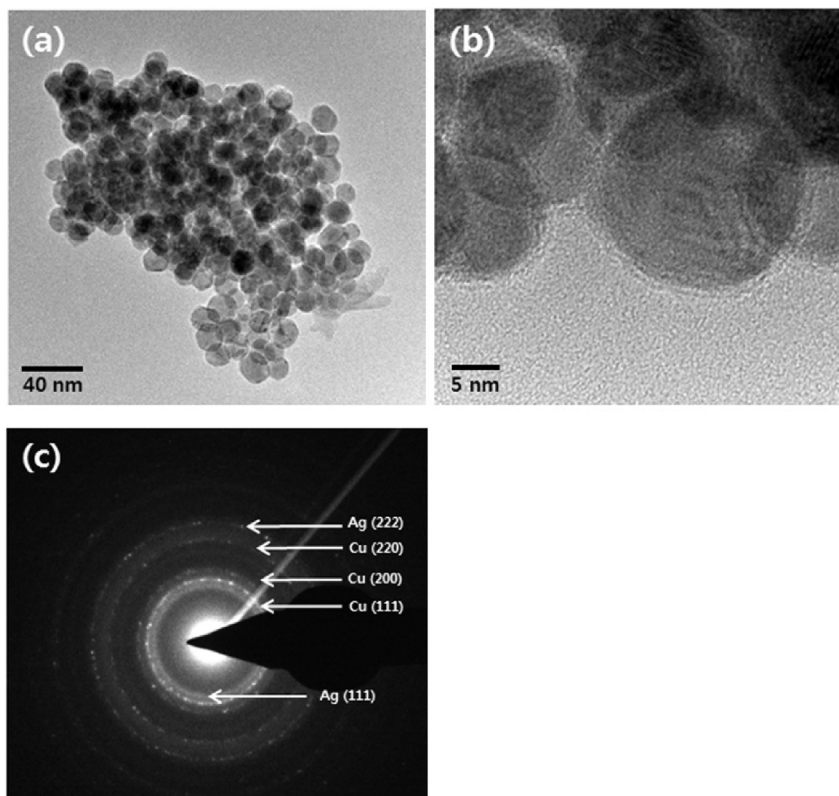


Fig. 1. (a, b) TEM images and (c) SEAD pattern of Cu@Ag NPs synthesized for 2 h at 150 °C with a Cu:Ag atomic ratio of 4:1.

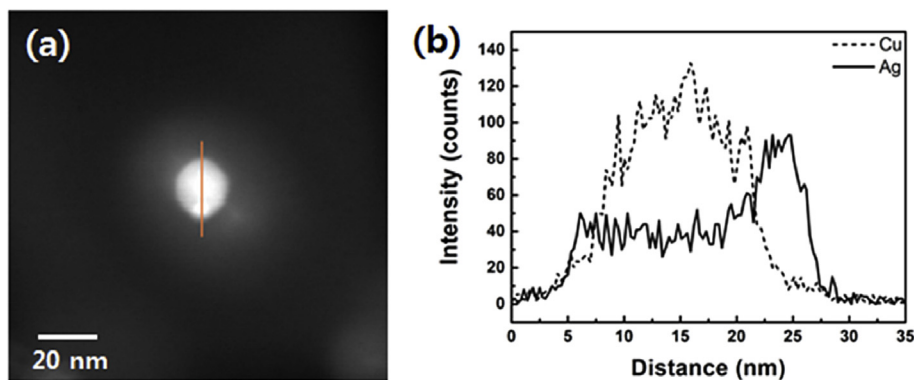


Fig. 2. STEM image and elemental line profiles of Cu@Ag NPs synthesized for 2 h at 150 °C with Cu:Ag atomic ratio of 4:1.

be achieved with the initial Cu:Ag atomic ratio of 4:1.

XRD results of the Cu@Ag NPs synthesized with different initial Cu:Ag atomic ratios are presented in Fig. 6. Considering two main peaks, the intensities of Ag (111) peaks seem to increase gradually and vice versa for those of Cu (111) with decreasing Cu:Ag atomic ratio. However, accurate amount ratios between Cu and Ag in Cu@Ag NPs can be obtained with the EDS results of Fig. 7. Fig. 7(a) shows the experimental amount ratios between Cu and Ag in Cu@Ag NPs synthesized for 2 h at 150 °C with different initial Cu:Ag atomic ratios. The amount ratios were determined by the ratio between areas formed by each main peak for Cu and Ag in the EDS measurement in the images of Fig. 5. In the cases where the initial Cu:Ag atomic ratio was 5:1 or 4:1, the amount ratios of Cu:Ag in the final Cu@Ag NPs were close to 5:1 or 4:1, respectively. In the case where the initial Cu:Ag atomic ratio was 3:1, however, the ratio in

the final NPs approached 4:1. This result can be inferred from the formation of fine pure Ag NPs, as shown in the low-magnification TEM image of Fig. 7(b). Although some free Ag NPs existed in the sample, the Ag was not measured in the magnified image of Fig. 5(d). Thus, the intensity of Ag peak in Fig. 5(d) diminishes, and value in the experimental amount ratio of Cu/Ag becomes higher than that of initial atomic ratio in this case. The EDS results indicate again that the thickest and most uniform Ag shell can be formed without the formation of fine pure Ag NPs when the initial Cu:Ag atomic ratio is 4:1.

Fig. 8 presents TEM images and fast FFT patterns of Cu₄@Ag₁ NPs annealed on the grid for 30 min at different temperatures. During the annealing at 200 °C [Fig. 8(a)], some bumps formed on the Cu₄@Ag₁ NP surfaces. The bumps were indexed to pure Ag by FFT patterns such as that shown in Fig. 8(b). It has been reported that

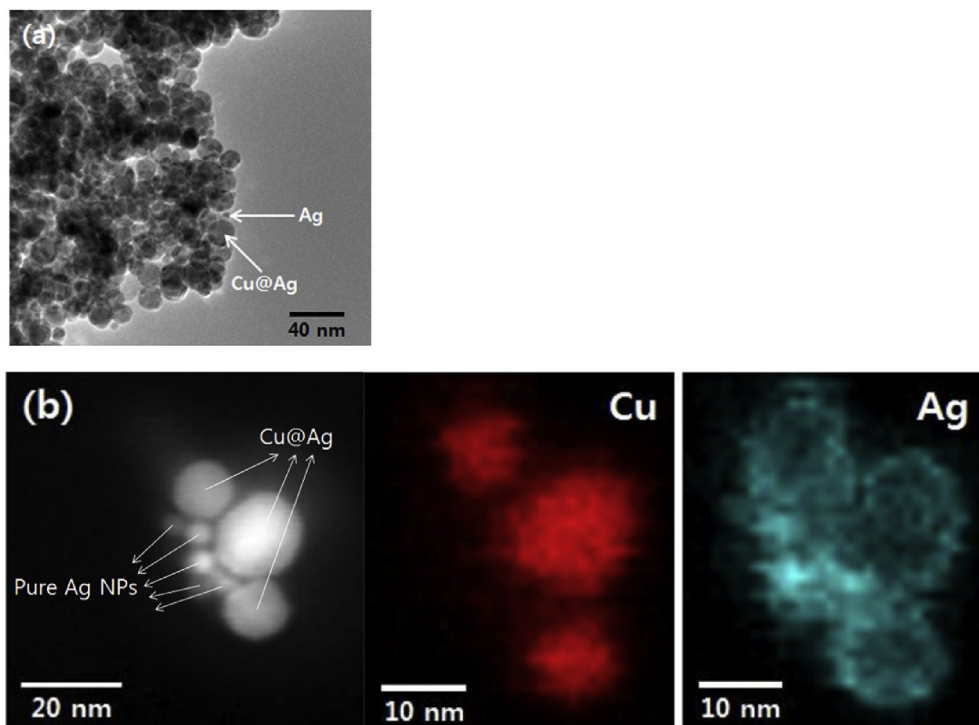


Fig. 3. (a) TEM and (b) elemental mapping images of Cu@Ag NPs synthesized for 2 h at 150 °C with Cu:Ag atomic ratio of 2:1.

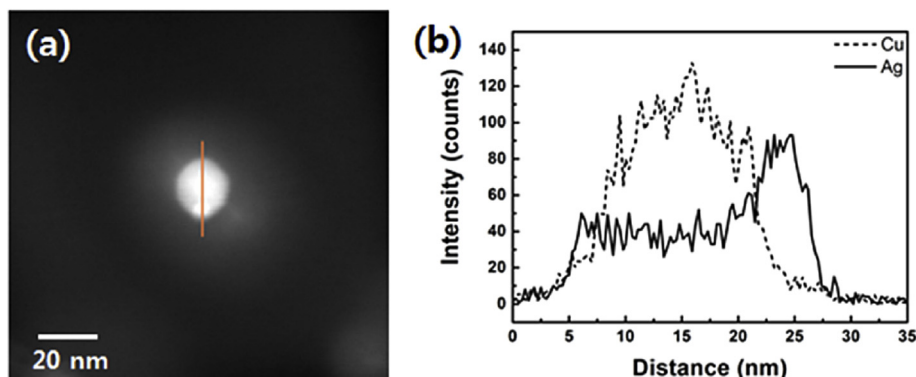


Fig. 4. (a) STEM image and (b) elemental line profiles of Cu@Ag NPs synthesized for 2 h at 150 °C with Cu:Ag atomic ratio of 2:1.

the Ag bumps are formed owing to the dewetting phenomenon of the Ag layers [12–14]. During the annealing at 250 °C [Fig. 8(c) and (d)], meanwhile, free Ag NPs were also observed together with the Ag bumps. Therefore, it was inferred from the images that the Ag bumps are transformed into free Ag NPs what destroys locally the Ag shell at the final stage of dewetting. The destruction of the Ag shell through the formation of free Ag NPs can lead to the abrupt surface oxidation of core Cu in Cu@Ag NPs [17]. The FFT pattern [inset of Fig. 8(c)] clearly indicates Cu oxidation in Cu@Ag NPs. The OA chemically capped on the Cu@Ag NPs is squeezed out during the annealing with the progress of sintering among metallic NPs by heating, finally forming assembly of OA such as cluster. The clusters of OA were thus observed with ease such as the zone indicated by dotted circles in the image of Fig. 8(d).

The elemental mapping images of Cu₄@Ag₁ NPs annealed on the grid for 30 min at 250 °C is shown in Fig. 9. The Ag shells worked loose overall and the density on the shell position decreased significantly. Furthermore, the strongest point in the Ag mapping

was located in the spaces among the Cu core NPs. This image presents sufficiently the Ag dewetting phenomenon and the destruction of Ag shells occurred during the annealing with the elemental analysis in high-magnification. With the progress of annealing, the oxidation of Cu core particles may proceed through the local destruction of Ag shells and the formation of loose Ag shells.

SEM images of film surfaces formed by sintering Cu₄@Ag₁ inks for 30 min at different temperatures are shown in Fig. 10. It was observed clearly from the particle growth that the sintering proceeded increasingly with increasing temperature. At the early stage of sintering, the numerous tiny voids among the particles disappeared via agglomeration between the particles. The remaining large voids were also increasingly removed as the temperature increased from 240 [Fig. 10(e)] to 300 °C [Fig. 10(f)]. When judged by the results of Figs. 8 and 9, however, the samples of Fig. 10(e) and (f) would be definitely oxidized.

Fig. 11 presents the electrical resistivities of films formed by

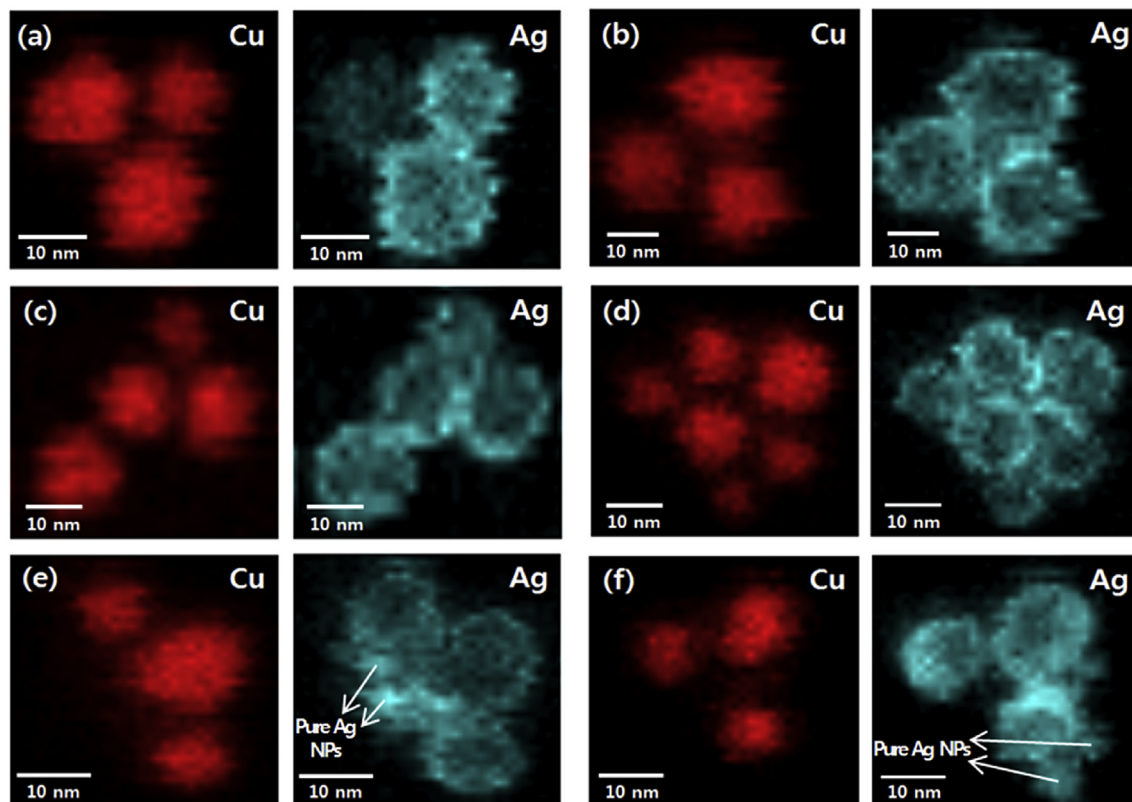


Fig. 5. Elemental mapping images of Cu@Ag NPs synthesized for 2 h at 150 °C with different Cu:Ag atomic ratios: (a) 6:1, (b) 5:1, (c) 4:1, (d) 3:1, (e) 2:1, and (f) 1:1.

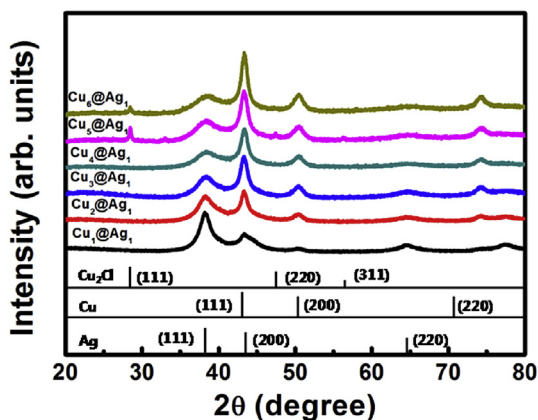


Fig. 6. XRD patterns of Cu@Ag NPs synthesized for 2 h at 150 °C with different Cu:Ag atomic ratios.

sintering Cu₄@Ag₁ inks for 30 or 60 min with respect to temperature in N₂ or air atmosphere. In order to suppress the oxidation of Cu₄@Ag₁ NPs, the sintering was carried out within 250 °C. The average final thickness of the sintered films was 1.7 μm. The Cu@Ag NPs used in Fig. 11(b) were washed with acetic acid prior to the ink fabrication to remove the chemically capped OA. In the case where the film was sintered for 60 min in nitrogen using the ink containing non-washed Cu₄@Ag₁ NPs [Fig. 11(a)], the resistance at 200 °C was abnormally high, but the resistance rapidly decreased with increasing temperature. As a result, the resistance at 240 °C was $2.70 \times 10^{-3} \Omega \text{ cm}$, which is lower than that of the film sintered in air using washed Cu₄@Ag₁ NPs under identical conditions. In the cases where the films were sintered in air after the washing

[Fig. 11(b)], electrical resistivity similarly decreased with a low slope when temperature was raised. Also, the increase of sintering time at the same temperature evidently induced a decrease of resistivity. As a representative value, the resistivity after sintering for 60 min at 240 °C in air was $4.96 \times 10^{-3} \Omega \text{ cm}$, which is similar to the value obtained when Cu NPs with a size of $45 \pm 8 \text{ nm}$ were sintered in vacuum under similar temperature and time [18]. In the present study, the films prepared from Cu NPs without Ag coating became discolored and high resistivities exceeding $10^2 \Omega \text{ cm}$ were measured after the air sintering, indicating that Cu was severely oxidized in the films. These results thus confirm the anti-oxidation properties of the Cu₄@Ag₁ NPs under air. A comparison of the results in Fig. 11(a) and (b) indicates that the chemically capped OA reduced sintering behavior among the metallic NPs under the case sintering temperature is not high enough. However, the resistances obtained after sintering for 60 min at 240 °C demonstrate the following two points: one, the increase of temperature rapidly reduce the sintering inhibition of the capped OA through the squeezing out and cluster formation, and two, the surfaces of Cu₄@Ag₁ NPs sintered at 240 °C shown in Fig. 11(b) were slightly oxidized, which increased the resistance value. In other words, the resistance values after sintering at 240 °C were influenced more by oxidation after Ag dewetting than by the capped OA.

4. Conclusions

Ultrafine Cu_x@Ag₁ NPs less than 20 nm in size were prepared under N₂ bubbling using a solvothermal method for the synthesis of core Cu NPs and an immersion-coating process to prepare an Ag shell on the Cu NPs. The fabrication conditions of Cu_x@Ag₁ NPs were optimized to reduce the fabrication of fine pure Ag NPs and to maximize the formation of thick and dense Ag shells. Then the Ag

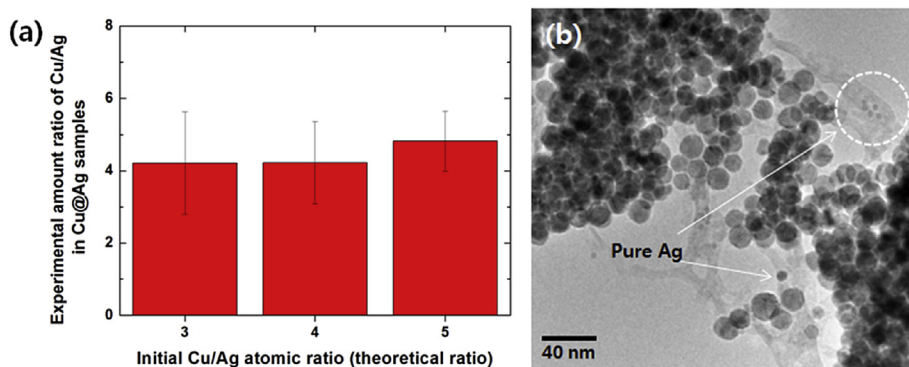


Fig. 7. (a) Experimental amount ratios of Cu:Ag in Cu@Ag NPs synthesized for 2 h at 150 °C with different initial Cu:Ag atomic ratios and (b) TEM image of Cu@Ag NPs synthesized based on Cu:Ag atomic ratio of 3:1.

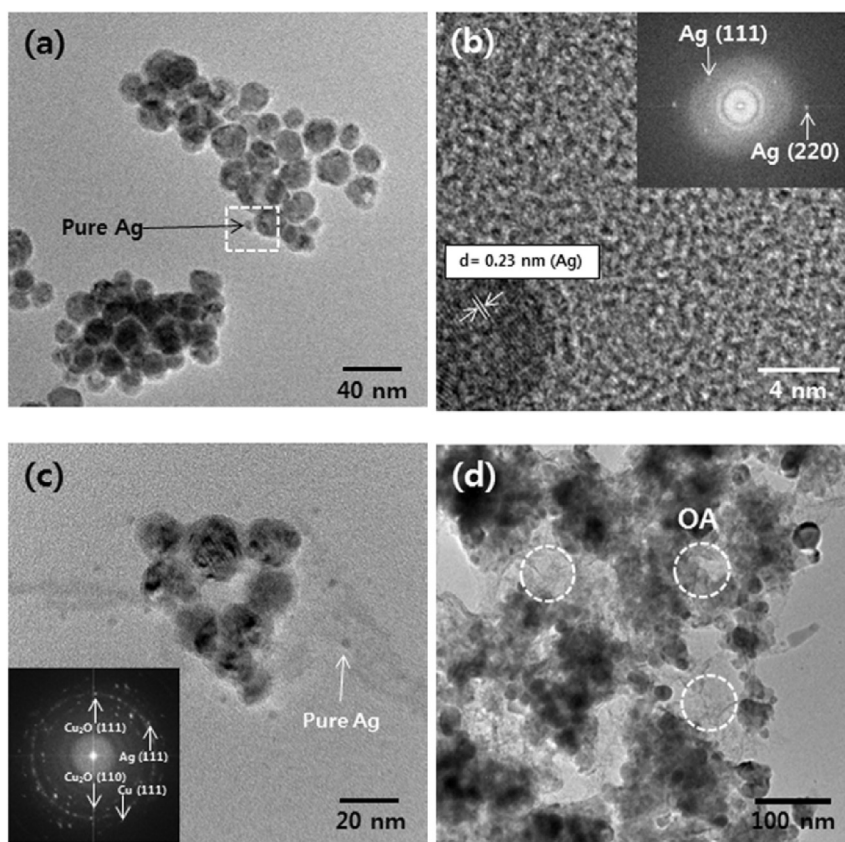


Fig. 8. TEM images and FFT patterns of Cu₄@Ag₁ NPs annealed for 30 min at different temperatures: (a, b) 200 and (c, d) 250 °C.

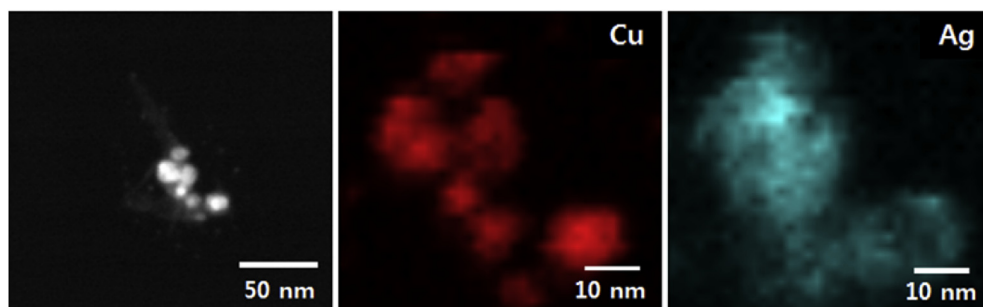


Fig. 9. Elemental mapping images of Cu₄@Ag₁ NPs annealed for 30 min at 250 °C.

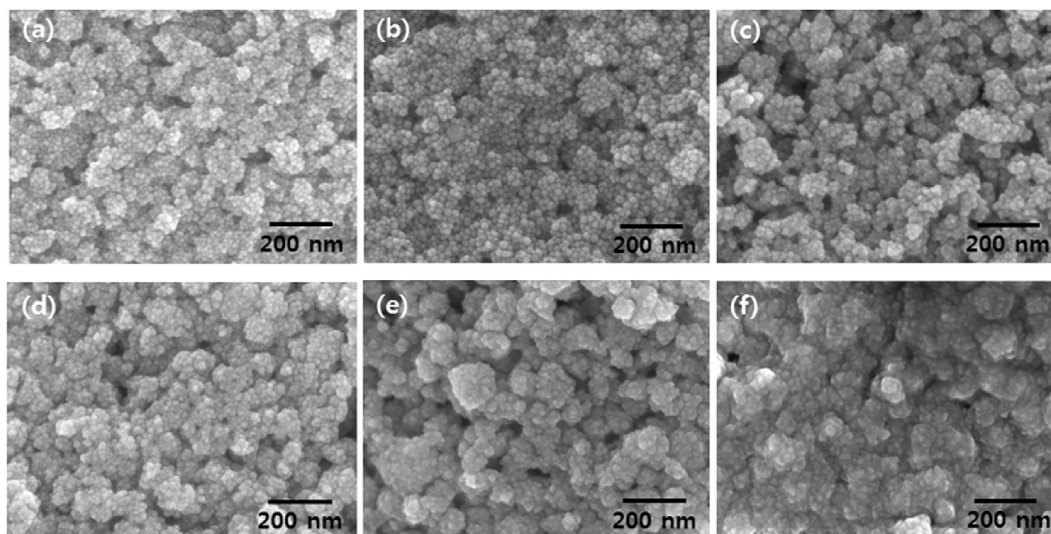


Fig. 10. SEM images of film surfaces formed by sintering $\text{Cu}_4\text{@Ag}_1$ inks for 30 min at different temperatures: (a) room temperature, (b) 180, (c) 200, (d) 220, (e) 240, and (f) 300 °C.

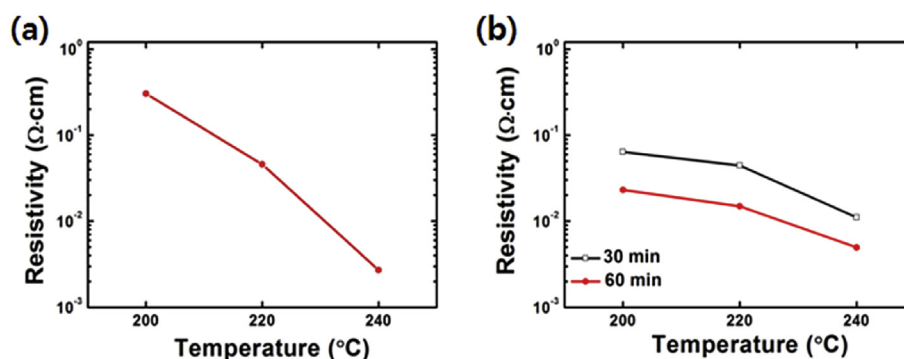


Fig. 11. Electrical resistivities with respect to temperature of $\text{Cu}_4\text{@Ag}_1$ films sintered for (a) 60 min in N_2 atmosphere or (b) 30 or 60 min in air with core-shell NPs washed with acetic acid.

dewetting behavior and Cu oxidation were analyzed with samples of the $\text{Cu}_4\text{@Ag}_1$ NPs, and the electrical resistivities of sintered $\text{Cu}_4\text{@Ag}_1$ films were measured as a function of sintering temperature. It was found that the Ag dewetting behavior occurred during heating at 200 °C and Cu oxidation was confirmed during heating at 250 °C. Nevertheless, the electrical resistivity gradually decreased with increasing temperature from 200 to 240 °C. The resistivity after washing the OA and sintering for 60 min at 240 °C in air was $4.96 \times 10^{-3} \Omega \text{ cm}$. This result confirmed the anti-oxidation properties of the $\text{Cu}_4\text{@Ag}_1$ NPs. The film was sintered under identical conditions in nitrogen using the ink containing non-washed $\text{Cu}_4\text{@Ag}_1$ NPs presented the lower resistivity of $2.70 \times 10^{-3} \Omega \text{ cm}$, although the values were relatively high under the case sintering temperature is not high enough because the capped OA on core-shell NPs hindered the sintering behavior.

Acknowledgments

This work was supported by the Materials & Components Technology Development Program (10047681, development of low cost conductive paste capable of fine pattern for touch panel and high conductivity for solar cell using metal composite with core-shell structure prepared by highly productive wet process) funded by the Ministry of Trade, Industry and Energy, Republic of Korea. The authors also thank Korean Basic Science Institute (KBSI) for the TEM, STEM, and XRD analyses.

References

- [1] A. Kamyshny, M. Ben-Moshe, S. Aviezer, S. Magdassi, *Macromol. Rapid Commun.* 26 (2005) 281–288.
- [2] A.L. Dearden, P.J. Smith, D.Y. Shin, N. Reis, B. Derby, P. O'Brien, *Macromol. Rapid Commun.* 26 (2005) 315–318.
- [3] Y. Sun, Y. Yin, B.T. Mayers, T. Herrecks, Y. Xia, *Chem. Mater.* 14 (2002) 4736–4745.
- [4] D. Zhang, L. Qi, J. Yang, J. Ma, H. Cheng, L. Huang, *Chem. Mater.* 16 (2004) 872–876.
- [5] W. Shen, X. Zhang, Q. Huang, Q. Xu, W. Song, *Nanoscale* 6 (2014) 1622–1628.
- [6] Y. Li, C.P. Wong, *Mater. Sci. Eng. R* 51 (2006) 1–35.
- [7] W. Li, M. Chen, J. Wei, W. Li, C. You, *J. Nanopart. Res.* 15 (2013) 1949.
- [8] Y.H. Kim, D.K. Lee, B.G. Jo, J.H. Jeong, Y.S. Kang, *Colloids Surf. A* 284 (2006) 364–368.
- [9] X. Xu, X. Luo, H. Zhuang, W. Li, B. Zhang, *Mater. Lett.* 57 (2003) 3987–3991.
- [10] J. Zhao, D. Zhang, J. Zhao, *J. Solid State Chem.* 184 (2011) 2339–2344.
- [11] C.K. Kim, G.J. Lee, M.K. Lee, C.K. Rhee, *Powder Technol.* 263 (2014) 1–6.
- [12] M. Grouchko, A. Kamyshny, S. Magdassi, *J. Mater. Chem.* 19 (2009) 3057–3062.
- [13] A. Muzikansky, P. Nanikashvili, J. Grinblat, D. Zitoun, *J. Phys. Chem. C* 117 (2013) 3093–3100.
- [14] H.T. Hai, H. Takamura, J. Koike, *J. Alloys Compd.* 564 (2013) 71–77.
- [15] R. Zhang, W. Lin, K. Lawrence, C.P. Wong, *Int. J. Adhes. Adhes.* 30 (2010) 403–407.
- [16] H. Nishikawa, S. Mikami, K. Miyake, A. Aoki, T. Takemoto, *Mater. Trans.* 51 (2010) 1785–1789.
- [17] S.S. Chee, J.H. Lee, *J. Mater. Chem. C* 2 (2014) 5372–5381.
- [18] B.K. Park, D. Kim, S. Jeong, J. Moon, J.S. Kim, *Thin Solid Films* 515 (2007) 7706–7711.